FEBS Letters 581 (2007) 462–468

Solution structure of an atypical WW domain in a novel β-clam-like dimeric form

Satoshi Ohnishi[a], Peter Güntert[a], Seizo Koshiba[a], Tadashi Tomizawa[a], Ryogo Akasaka[a], Naoya Tochio[a], Manami Sato[a], Makoto Inoue[a], Takushi Harada[a], Satoru Watanabe[a], Akiko Tanaka[a], Mikako Shirouzu[a], Takanori Kigawa[a,b], Shigeyuki Yokoyama[a,c,*]

[a] *Genomic Sciences Center, RIKEN, 1-7-22 Suehiro-cho, Tsurumi, Yokohama 230-0045, Japan*
[b] *Department of Computational Intelligence and Systems Science, Interdisciplinary Graduate School of Science and Engineering, Tokyo Institute of Technology, 4259 Nagatsuta-cho, Midori-ku, Yokohama 226-8503, Japan*
[c] *Department of Biophysics and Biochemistry, Graduate School of Science, University of Tokyo, 7-3-1 Hongo, Bunkyo-ku, Tokyo 113-0033, Japan*

Received 13 November 2006; revised 2 January 2007; accepted 8 January 2007

Available online 16 January 2007

Edited by Miguel De la Rosa

Abstract **The WW domain is known as one of the smallest protein modules with a triple-stranded β-sheet fold. Here, we present the solution structure of the second WW domain from the mouse salvador homolog 1 protein. This WW domain forms a homodimer with a β-clam-like motif, as evidenced by size exclusion chromatography, analytical ultracentrifugation and NMR spectroscopy. While typical WW domains are believed to function as monomeric modules that recognize proline-rich sequences, by using conserved aromatic and hydrophobic residues that are solvent-exposed on the surface of the β-sheet, this WW domain buries these residues in the dimer interface.**

Keywords: NMR; WW domain; Homodimer; Salvador homolog 1 protein

1. Introduction

The WW domain is known as a small protein module, composed of 30–40 amino acids, that folds into a monomeric, triple-stranded, anti-parallel β-sheet, without the assistance of disulfide bonds or metal chelation. Its small size and compact fold have drawn attention for studies of protein folding, stability and design [1–5]. It typically has two conserved tryptophan residues spaced 20–23 amino acids apart (and thus is called the WW domain), and one conserved proline residue located three residues after the second conserved tryptophan. WW domains usually recognize various proline-rich sequences by using conserved aromatic and hydrophobic residues that are exposed on the surface of the β-sheet. The amino acid pattern of these conserved residues determines the specificity of the proline-rich ligands, which has allowed the classification of WW domains into four groups [6–8].

Eukaryotic salvador (*sav*) was recently identified as an important gene that promotes both cell cycle exit and apoptosis [9]. The *sav*1 gene from mouse encodes the salvador homolog 1 protein with 386 amino acid residues. The protein sequence was predicted to contain three structural domains on the Swiss-Prot database [10] (primary accession number: Q8VEB2): two WW domains in the middle, followed by the C-terminal SARAH domain, which has a coiled-coil motif (Fig. 1A). The sequence homology between these two WW domains is not high (identity = 37.1%, positives = 71.4%, Fig. 1B), suggesting a difference in their functional roles. According to a sequence-based prediction of the ligand-binding specificity [6–8], the first WW domain of the salvador homolog 1 protein is classified into the Group I WW domain, which interacts with the PPXY (''PY'') motif. In contrast, the second WW domain has a tyrosine substitution of the second conserved tryptophan residue that plays a key role in ligand binding, and therefore, its functional role may differ from those of the canonical WW domains [11,9] (Fig. 1B). In addition, the same tyrosine substitution is conserved between the second WW domains in orthologues of the salvador homolog 1 protein, suggesting the unique role of this atypical WW domain (Fig. 1C).

In this study, we have determined the three-dimensional structure of the second WW domain from the mouse salvador homolog 1 protein (mSAV1 WW_2) by solution NMR spectroscopy. Notably, this WW domain forms a homodimer with a β-clam-like motif. This is the first discovery of a WW domain that is capable of forming a dimer. We provide evidence for the homodimer formation from different experimental techniques, and discuss the biological implications based on the present structure.

2. Materials and methods

2.1. Protein expression and purification

The DNA encoding the mouse SAV1 gene was subcloned by PCR from the mouse cDNA clone locus AAH19377 (Mouse Ultimate™ Full ORF Gateway(R) Shuttle Clones, Invitrogen, ID: IOM16694). The region between P231 and P266 was cloned into the expression vector pCR2.1 (Invitrogen) as a fusion with an N-terminal His6 affinity tag and a tobacco etch virus (TEV) protease cleavage site. The actual construct contains seven extra residues (GSSGSSG) after the TEV cleavage site and six extra residues at the C-terminus (SGPSSG) that are

*Corresponding author. Fax: +81 45 503 9195.
E-mail address: yokoyama@biochem.s.u-tokyo.ac.jp (S. Yokoyama).

Abbreviations: mSAV1 WW_2, the second WW domain of the mouse salvador homolog 1 protein

0014-5793/$32.00
doi:10.1016/j.febslet.2007.01.008

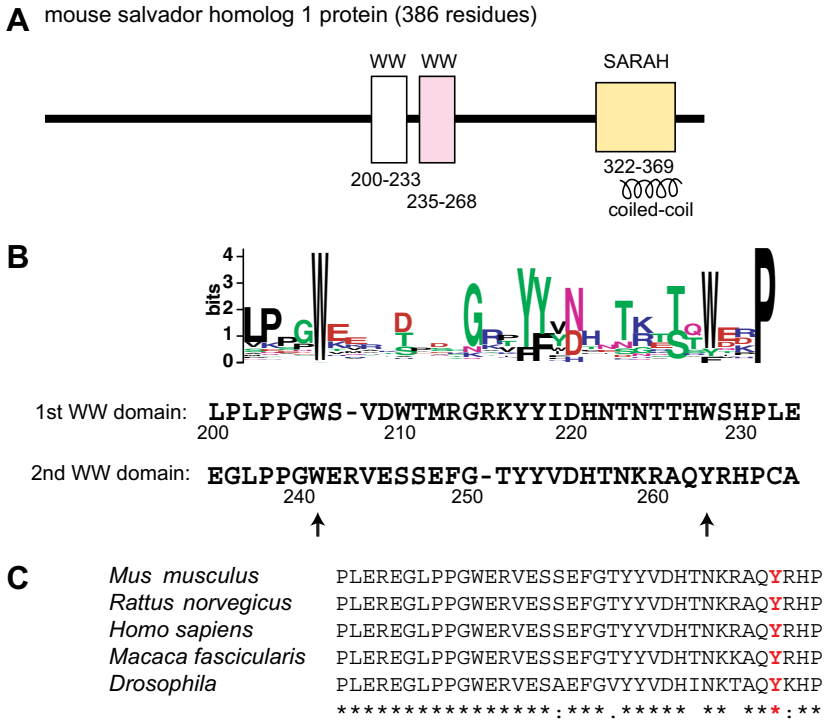

Fig. 1. (A) Predicted domain structure of the mouse salvador homolog 1 protein. The domain map is illustrated based on the prediction by the Swiss-Prot database [10]. (B) Comparative representation of the amino acid sequences of the first and second WW domains and the LOGO plot of the seed sequences of the WW domains defined by the Pfam database [35]. The numbers under the sequences correspond to the residue numbers in the full length salvador homolog 1 protein. The two conserved tryptophan sites are marked with arrows. (C) Sequence alignment of the second WW domain of the salvador homolog 1 protein from multiple organisms. The substitution at the second conserved tryptophan is marked in red.

derived from the expression vector. The fusion protein was synthesized by the cell-free protein expression system using $^{13}C/^{15}N$-labeled amino acids [12,13], and was purified using a chelating column, as described elsewhere [14]. The purified protein was concentrated to 1.2 mM in 20 mM d-Tris–HCl buffer (pH 7.0) containing 100 mM NaCl, 1 mM D-dithiothreitol, 10% D_2O and 0.02% NaN_3.

2.2. Analytical size exclusion chromatography

The size exclusion chromatography was carried out using an LC-10ADvp system (SHIMADZU, Kyoto, Japan) with a TSKgel $G2000SW_{XL}$ column (7.8 mm I.D. × 30 cm, TOSOH, Tokyo, Japan) that was pre-equilibrated with 20 mM sodium phosphate buffer (pH 6.0) containing 200 mM Na_2SO_4. A 10 μL aliquot of the purified WW domain sample was injected into the column, with a flow rate of 1.0 mL/min, and the elution was monitored by UV absorbance at both 215 and 280 nm.

2.3. Analytical ultracentrifugation

Sedimentation equilibrium experiments were performed using a Beckman Optima XL-I centrifuge. Experiments were carried out with 100 μl samples of the WW domain, at 0.4, 0.2, and 0.1 mg/ml concentrations in 20 mM Tris–HCl (pH 7.0), using six channel centerpieces. An 8-position rotor (An-50 Ti) was rotated for 16 h at 23000 rpm, 25000 rpm, and 27000 rpm. Data were collected after 12 h, 14 h, and 16 h at each speed, by monitoring the UV absorbance at 280 nm. The protein samples were then completely sedimented at 40000 rpm for 6 h, to generate the baseline. Data were analyzed using a partial specific volume of 0.6991 ml/g and a solvent density of 1.00293 g/ml to determine the molecular weight, using the XL-A/XL-I Data Analysis software, Ver. 6.03.

2.4. NMR spectroscopy

All spectra were recorded on Bruker Avance 600 and 800 spectrometers at 298 K. Resonance assignments were accomplished using a conventional set of triple resonance spectra, as described previously [14], and have been deposited in the Biological Magnetic Resonance data Bank (BMRB) (accession number: 10028). Interproton distance restraints were obtained from ^{15}N and ^{13}C edited NOESY spectra, both recorded with a mixing time of 150 ms. To identify the intermolecular NOE peaks, the ^{13}C filtered ^{13}C-edited NOESY spectrum [15] was recorded for the mixture of 1.0 mM ^{15}N–^{13}C-labeled protein and 1 mM non-labeled protein, in 20 mM d-Tris–HCl buffer (pH 7.0) containing 100 mM NaCl and 99.9% D_2O. All spectra were processed using NMRPipe [16], and the programs Kujira [N. Kobayashi, personal communication] and NMRView [17] were employed for optimal visualization and spectral analyses.

2.5. Collection of conformational restraints, structure calculation and refinement

Automated NOE cross-peak assignments [18] and structure calculations with torsion angle dynamics [19] were performed using a modified version of the program CYANA 2.1 [20,21], which takes the homodimer symmetry explicitly into account for the network-anchoring of the NOE assignments [18]. In the process of the structural solution, torsion angle difference restraints on all corresponding torsion angles were imposed to ensure the identical conformation of the two monomers. In addition, distance difference restraints between symmetry-related intermolecular C_α–C_α distances were applied to maintain a symmetric relative orientation of the two monomers. Backbone torsion angle restraints obtained from database searches with the program TALOS [22] were incorporated within the structural calculation. CYANA structure calculations were started from 100 randomized conformers, and simulated annealing with 20000 torsion angle dynamics time steps per conformer was performed. The 20 conformers with the lowest final CYANA target function values were subjected to restrained energy minimization in explicit solvent against the AMBER force field [23], using the program OPALp [24,25]. The protein was immersed in a shell of water molecules with a thickness of 8 Å. A maximum of 3000 steps of restrained conjugate gradient minimization were applied, using the standard AMBER force field and a pseudo-potential for NOE upper distance bounds that was proportional to the sixth

power of the restraint violation. The force constant was chosen such that a restraint violation of 0.1 Å contributed 0.9 kcal/mol to the potential energy. The structural quality was evaluated with PROCHECK-NMR [26], and the coordinates have been deposited in the Protein Data Bank database (PDB code: 2DWV). The program MOLMOL [27] was used to calculate the aromatic ring current shift effects and to visualize the structures.

3. Results and discussion

3.1. Hydrodynamic properties

The purified fraction of mSAV1 WW_2 showed a single peak on the size exclusion chromatography with a significantly shorter retention time than that expected from the theoretical molecular weight of a protein with 49 amino acid residues, suggesting possible dimer formation (Fig. 2A). The dimer formation of the present WW domain was confirmed by the high-speed sedimentation equilibrium study, using analytical ultracentrifugation. The radial distributions of the WW domain samples at various concentrations all fit well to a single exponential curve corresponding to a molecular weight of 11 863, while the theoretical value is 5592 (Fig. 2B). This suggests that the majority of the present WW domain is in a dimeric state. Since the WW domain is generally considered to be a monomeric protein module [28,8], this novel finding of dimer formation highlights the importance of the structural determination of the dimeric mSAV1 WW_2.

3.2. NMR spectroscopy and structural determination

As shown in Fig. 2C and D, mSAV1 WW_2 showed well-resolved HSQC spectra with a single set of resonance assignment, suggesting that it adopts a single conformer in solution. The chemical shifts, as well as the linewidths, were insensitive to the 24-fold dilution of the sample solution,

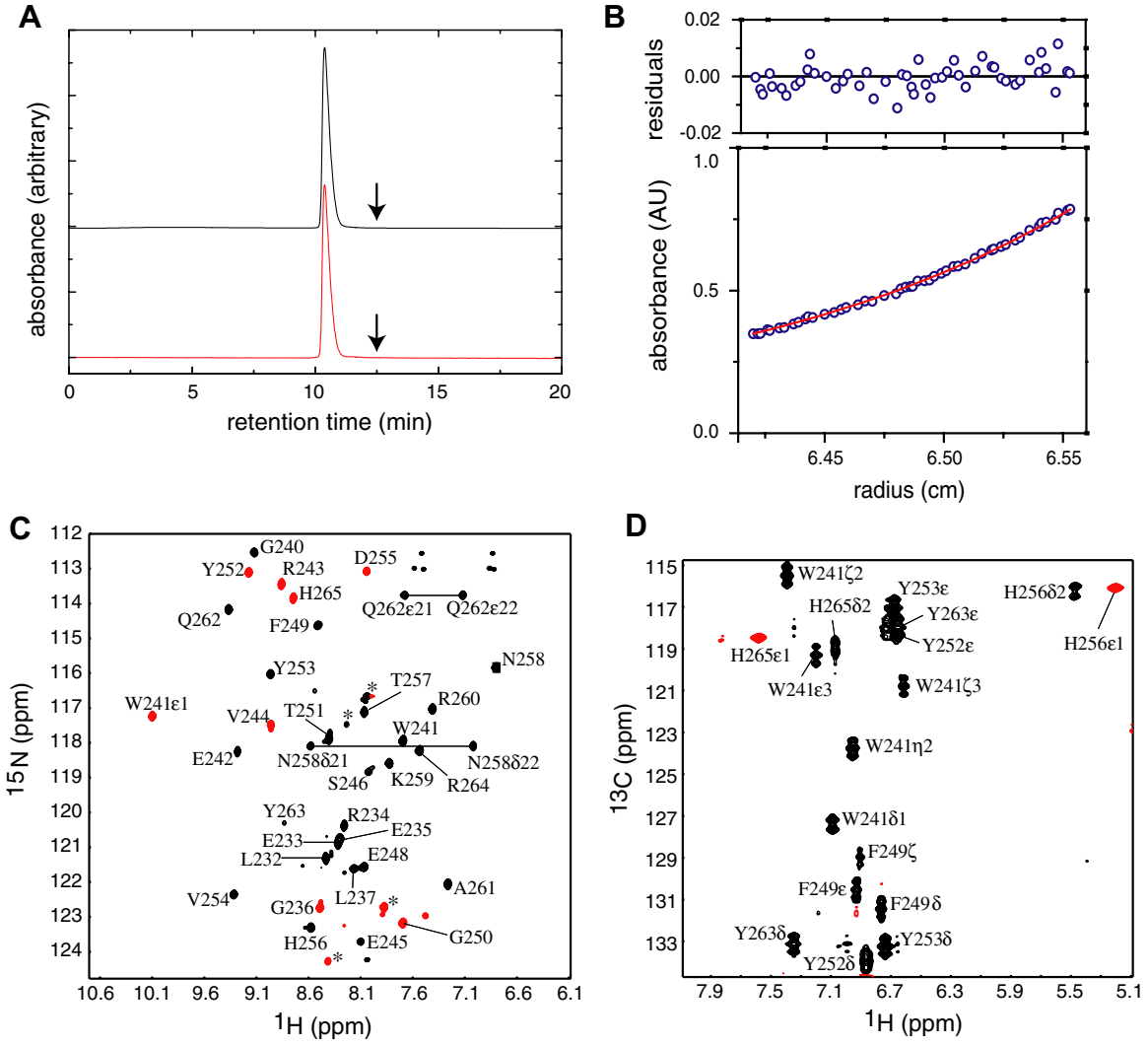

Fig. 2. (A) Size exclusion chromatography of mSAV1 WW_2, monitored by UV absorbance at 215 nm (black) and 280 nm (red). Arrows indicate predicted elution positions for a WW domain monomer. (B) Equilibrium analytical centrifugation of mSAV1 WW_2. The bottom panel shows the radial distribution of absorbance in the centrifuge cell at equilibrium at 25 000 rpm, with a protein concentration of 0.4 mg/ml. The red solid line through the data represents the fit to a single species with a molecular weight corresponding to 11 863 Da. The residuals for the fit are shown in the upper panel. (C) A ^{1}H–^{15}N HSQC spectrum of mSAV1 WW_2. Red signals represent folded peaks due to a narrow spectrum width. Peaks marked with * are signals from the residues in the artificial tags of the present construct. (D) A ^{1}H–^{13}C HSQC spectrum for the aromatic region of the present WW domain. Red signals represent folded peaks due to a narrow spectrum width.

suggesting that conformation of the present WW domain is independent from protein concentration, at least, for the range between 0.05 mM and 1.2 mM. We could assign 98.5% of all non-labile and backbone amide ^{1}H chemical shifts, excluding the artificial tail regions that are unstructured in solution.

The main challenge for the structure determination was the distinction between the intramolecular and intermolecular NOEs. We prepared an intermolecular NOE peak list from the ^{13}C-filtered ^{13}C-edited NOESY experiment [15], which was designed to selectively detect the NOEs from protons covalently attached to ^{12}C to a proton of interest that is attached to ^{13}C. This experiment was applied to the 1:1 mixture of the ^{15}N–^{13}C-labeled protein and the non-labeled protein, in which 50% was assumed to form a dimer between the labeled protein and the non-labeled protein, with 25% between the non-labeled proteins, and the rest between the labeled proteins. Thus, the ^{13}C-filtered experiment detects NOEs between ^{13}C-attached protons and ^{12}C-attached protons from the 50% fraction of the total dimeric molecules. In practice, it appears that the ^{13}C-filtered NOESY spectrum showed residual signals from intra-residue spin pairs due to incomplete isotope labeling, which could not be clearly discriminated from the intermolecular signals between symmetrically positioned residues. For example, Val254 is located in the center of the dimer interface, as revealed later, and the residual NOE signal between the intraresidual pairs of H_β and H_α of Val254 is indistinguishable from the signal between H_β of Val254 of molecule 1 and H_α of Val254 of molecule 2. Therefore, we did not select NOE peaks between intraresidual spin pairs but only unambiguously assigned intermolecular NOE cross peaks. The automated NOESY assignment algorithm of CYANA allowed only intermolecular assignments for these peaks, and assigned 61 out the 62 ^{13}C-filtered NOESY cross peaks. In contrast, both the intramolecular and intermolecular assignments were allowed for the cross peaks from the two conventional NOESY spectra. The initial ambiguity between the intramolecular and intermolecular assignment possibilities was represented by the ambiguous distance restraints [29]. Overall, 98.3% of all entries in the NOESY peak lists were assigned by CYANA, which yielded 150 intermolecular and 1432 meaningful intramolecular NOE distance restraints (Table 1). The 20 conformers with the lowest final CYANA target function values were further refined by restrained energy minimization in explicit solvent using OPALp [24,25]. The resulting 20 energy-minimized conformers represent the homodimeric structure of mSAV1 WW_2 (Fig. 3A). Disordered N- and C-terminal regions correspond to the extra residues coming from the expression vector.

The dimer structure of mSAV1 WW_2 is highly symmetric, and each molecule of the dimer exhibits a global fold with the triple-stranded antiparallel β-sheet, typical of the canonical WW domains (strand 1, W241–S246; strand 2, G250–D255; strand 3, R260–Q262) (Fig. 3). Most remarkably, the mSAV1 WW_2 dimer buries the conserved hydrophobic and aromatic residues that are important for ligand binding in the interface.

3.3. Factors that stabilize dimer formation

WW domains typically have conserved aromatic and hydrophobic residues exposed on the β-sheet that are used for ligand binding. In the case of the present WW domain, in contrast, these key residues are buried in the interface of the β-clam-like homodimer (Fig. 3C), which has not been reported in the

Table 1
NMR restraints and structure calculation statistics

Quantity	Value
NOE distance restraints	
Total	1582
Short-range ($\|i-j\| \leqslant 1$)	815
Medium-range ($1 < \|i-j\| < 5$)	217
Long-range ($\|i-j\| \geqslant 5$)	550
Intermolecular	150
Maximal violation (Å)	0.14
Torsion angle restraints	
ϕ	22
ψ	22
Maximal violation (°)	0.41
CYANA target function value (Å^2)	0.49 ± 0.15
AMBER energies (kcal/mol)	
Total	−3401 ± 128
van der Waals	−210 ± 15
Electrostatic	−3888 ± 127
Ramachandran plot (%)[a]	
Residues in most favored regions	79.3
Residues in additional allowed regions	19.9
Residues in generously allowed regions	0.8
Residues in disallowed regions	0.0
RMSD from the averaged coordinates (Å)[a]	
Backbone atoms	0.36
Heavy atoms	0.71

Where applicable, the value given corresponds to the average over the 20 energy-refined conformers that represent the solution structure. CYANA target function values were computed before energy refinement.
[a]For residues L237–P266 (dimer).

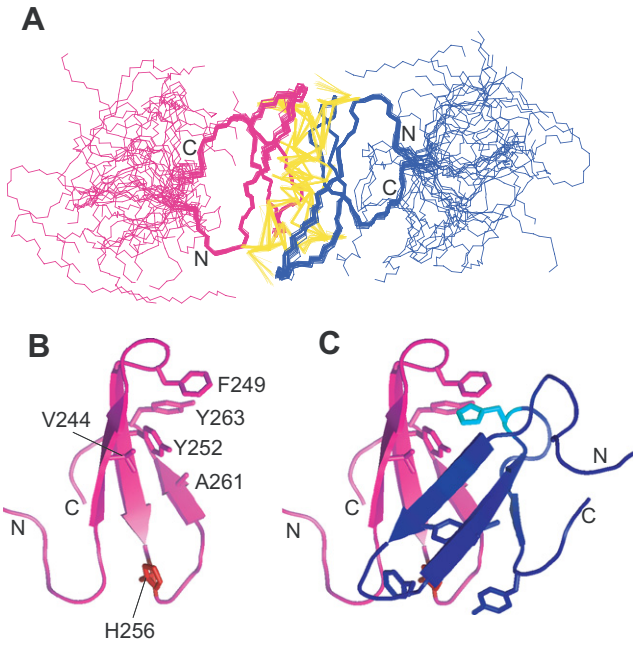

Fig. 3. (A) Superposition of the 20 energy minimized conformers that represent the structure of mSAV1 WW_2 in the β-clam-like homodimeric form. Yellow lines represent intermolecular distance constraints. The N- and C-termini are labeled. (B,C) A ribbon representation of one molecule of the WW domain dimer (B) and that of the dimer with the identical view angle (C). Key residues in the dimer interface are highlighted with a neon representation, and His256 is also highlighted. The N- and C-termini are labeled.

literature to date. A sequence alignment with 20 known WW domain entries from the PDB databank (Fig. 4A) suggested a few sites that may be responsible for the dimer formation: Val244 and Ala261 at the conserved hydrophilic sites, which both increase the hydrophobicity of the dimer interface; and the deletion between Gly250 and Thr251 that causes a bend in the turn between strand 1 and strand 2, which enables Phe249, at the conserved hydrophilic site, to form an aromatic pocket with Tyr252 and Tyr263 (Figs. 3B and 4B). A structural comparison with one of the canonical WW domains highlights the uniqueness of the twisted turn and the configuration of Phe249 (Fig. 4B). Presumably, this bend in the turn is linked to the formation of the aromatic pocket, which is one of the most critical factors for the dimer formation.

The substitution of the C-terminal conserved tryptophan by tyrosine (Tyr263) appears to be important for creating an aromatic pocket with a shape suitable for docking with the surface-exposed histidine (His256) of the other molecule (Fig. 3C). However, this substitution by itself is not directly linked to the dimer formation, since some PDB entries that lack the second conserved tryptophan represent monomeric WW domain structures (1TK7, 1WMV, and 2DJY). Notably, the aromatic packing at the interface is most supported by the unusual upfield resonance shifts of $H_{\delta 2}$ (5.47 ppm) and $H_{\varepsilon 1}$ (5.20 ppm) of His256 (Fig. 2D), while the chemical shift values of $H_{\delta 2}$ and $H_{\varepsilon 1}$ of histidine, derived from the BMRB statistics, are on average 7.07 ppm and 8.00 ppm, respectively. Aberrant downfield resonance shifts of histidine imidazole protons over 1.5 ppm deviation from the average values have been reported for some proteins, where these imidazole protons are involved in tight hydrogen bonds [30,31]. In contrast, unusual upfield resonance shifts of the imidazole protons of His256 can be well explained by ring current shifts upon immobilization of this imidazole ring into the aromatic pocket formed with Phe249, Tyr252, and Tyr263 (Fig. 3B and C). Using the 20 energy-refined dimer conformers, the ring current shifts of $H_{\delta 2}$ and $H_{\varepsilon 1}$ of His256 were calculated up to −2.3 ppm and −2.1 ppm, respectively, while only negligible ring current shifts, of up to −0.15 ppm for $H_{\delta 2}$ and −0.05 ppm for $H_{\varepsilon 1}$, were obtained, based on the hypothetical monomeric form, in which the side-chain of His256 is exposed to the solvent (Fig. 3B). The BMRB database contains chemical shift data for six WW domains that have a histidine in the equivalent sequence position. Their aromatic chemical shift values are in the ranges of 6.04–7.13 ppm for $H_{\delta 2}$ and 6.74–8.30 ppm for $H_{\varepsilon 1}$. This highlights the peculiarity of the present case, and suggests that the present WW domain forms a homodimer, while the other WW domains are monomeric.

The imidazole chemical shifts of His256 were 240.43 ppm for $^{15}N_{\delta}$ and 160.78 ppm for $^{15}N_{\varepsilon}$, respectively, suggesting that this histidine, buried in the dimer interface, adopts the $N^{\varepsilon 2\text{-}H}$ tautomer [32]. Since histidine is an ionisable residue, it is of great interest to examine effect of pH on the stability of the dimer with the histidine embedded interface. As shown in Fig. 5A,

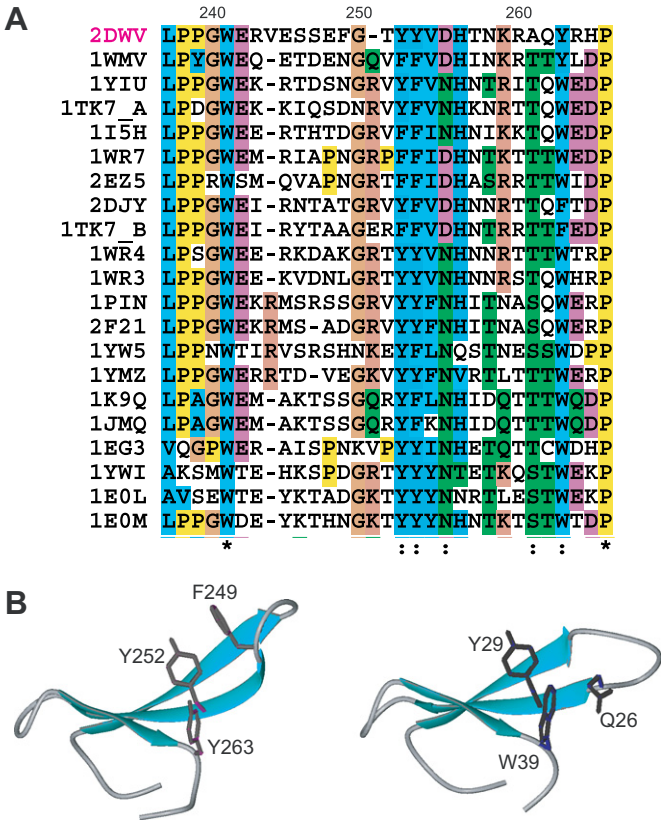

Fig. 4. (A) Sequence alignment of mSAV1 WW_2 (2DWV) with 20 canonical WW domains that were arbitrarily selected from the PDB databank. The numbers above the sequences correspond to the residue number of the present WW domain in the full length salvador homolog 1 protein. (B) Comparison between the mSAV1 WW_2 structure (left) and that of one canonical WW domain (1K9Q) (right). The side chains of Phe249, Tyr252, and Tyr263 in the present WW domain, as well as those of their counterparts (Gln26, Tyr29, and Trp39) in the canonical WW domain, are highlighted with a neon representation.

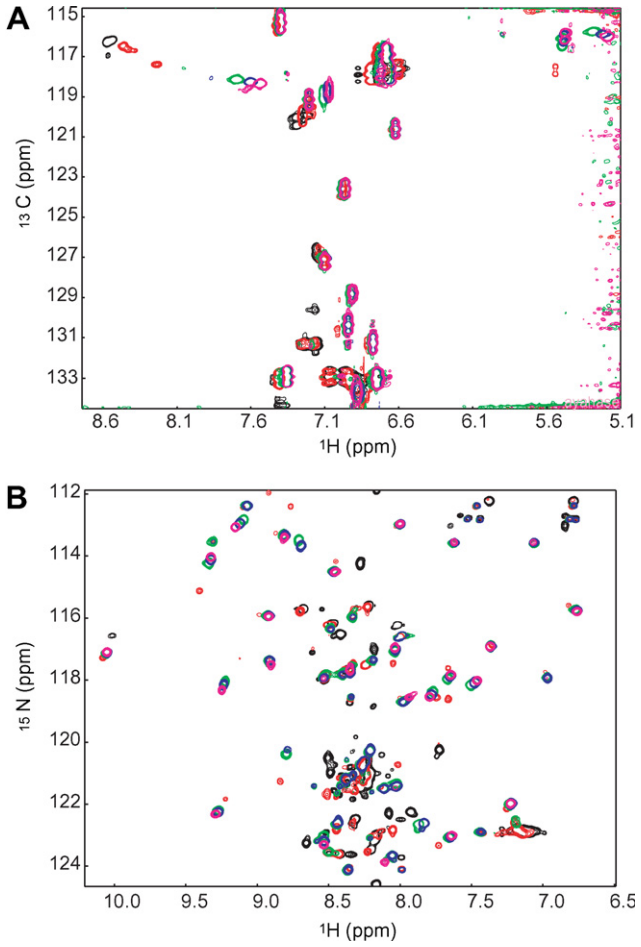

Fig. 5. HSQC spectra of mSAV1 WW_2 recorded at various pHs. The $^{1}H–^{13}C$ HSQC spectra for the aromatic region (A) and the $^{1}H–^{15}N$ HSQC spectra (B) were recorded at pH 8.8 (magenta), 6.9 (blue), 6.4 (green), 5.5 (red), and 4.4 (black). These pH values represent direct pH readings of the samples that contain 10% D_2O.

the abnormal imidazole resonances of His256 were little perturbed by changing pH from 8.8 to 6.4. In contrast, at pH 4.4, they became typical for the imidazole resonances of protonated histidine ($H_{\delta 2} \sim 7.2$ ppm, $C_{\delta 2} \sim 131$ ppm, $H_{\varepsilon 1} \sim 8.6$ ppm, $C_{\varepsilon 1} \sim 136$ ppm) [31]. This acidic sample became slightly turbid over time, and the $^{1}H–^{15}N$ HSQC peaks of this sample were collapsed around ~8.3 ppm (Fig. 5B), suggesting that the protein is denatured at this pH. At pH 5.5, two resonance sets, that are indicative of the homodimeric form and the acid denatured form, were observed both in the $^{1}H–^{13}C$ aromatic HSQC spectrum and the $^{1}H–^{15}N$ HSQC spectrum (Fig. 5). Thus, stability of the mSAV1 WW domain homodimer is pH dependent, which is linked to the ionization state of His256. Although typical WW domains are usually stable in the monomeric state, it is likely that the monomeric form of the present WW domain is unstable, as dissociation of the homodimeric form results in the denaturation of the WW domain.

3.4. Biological implications

As shown in Fig. 1A, the salvador homolog 1 protein has two tandem WW domains. A previous study reported that the *sav* gene regulates cell numbers in cooperation with another gene, *wts*, and that the salvador homolog 1 protein interacts with the *wts*-encoded protein, the serine/threonine-protein kinase LATS1 [9]. The first WW domain is predicted to belong to the Group I WW domain that specifically recognizes the "PY" motif [6–8], which occurs twice in the mouse LATS1 protein. A pull-down assay demonstrated that the region containing the two WW domains of the salvador homolog 1 protein interacts with the mouse LATS1 protein, and that the interaction was inhibited by the addition of a peptide derived from the PY motifs of the LATS1 protein [9]. Moreover, this inhibition was lost by the replacement of the tyrosine residue of the PY motif peptide that is required for the interaction with the Group I WW domains [9]. Therefore, the first WW domain is probably responsible for the interaction with the LATS1 kinase. In contrast, the second WW domain forms a homodimer using the peptide-binding site as the dimer interface, and therefore it is unlikely to interact with other protein molecule(s). The characteristic sequence pattern in this atypical WW domain that is probably responsible for the dimer formation is conserved among the orthologous proteins (Fig. 1C). Moreover, orthologues of the full-length salvador homolog 1 protein show the greatest degree of conservation in the region spanning from the second WW domain to the C-terminal end, and a coiled-coil motif that serves as the self-association interface is predicted in the downstream region of the second WW domain (Fig. 1A). Taken together, these observations led to the hypothesis that the salvador homolog 1 protein self-associates in the functional form, and this is facilitated by its atypical WW domain.

Recently, Hippo, the Drosophila homologue of the mammalian Ste20-like kinases MST1/MST2, was also found to interact with the salvador protein from Drosophila during the regulation of cell proliferation and apoptosis [33]. The C-terminal 60 residues of Hippo reportedly dimerize [34], and an immunoprecipitation study revealed that the C-terminal domain of the Drosophila salvador protein, which corresponds to the SARAH domain in the mammalian salvador homolog 1 protein (Fig. 1A), binds to the dimerization domain of Hippo [33]. These results suggest that the salvador protein may act as a scaffold to assemble signaling complexes comprising the Hippo and LATS kinases, which is consistent with the above hypothesis.

Acknowledgements: We thank M. Sato, Y. Ide, M. Kato, A. Hiyoshi and S. Morita for sample preparation. This work was supported by the RIKEN Structural Genomics/Proteomics Initiative (RSGI) and by the National Project on Protein Structural and Functional Analyses, Ministry of Education, Culture, Sports, Science and Technology of Japan.

References

[1] Crane, J.C., Koepf, E.K., Kelly, J.W. and Gruebele, M. (2000) Mapping the transition state of the WW domain beta-sheet. J. Mol. Biol. 298, 283–292.
[2] Deechongkit, S., Nguyen, H., Powers, E.T., Dawson, P.E., Gruebele, M. and Kelly, J.W. (2004) Context-dependent contributions of backbone hydrogen bonding to beta-sheet folding energetics. Nature 430, 101–105.
[3] Jager, M., Nguyen, H., Crane, J.C., Kelly, J.W. and Gruebele, M. (2001) The folding mechanism of a beta-sheet: the WW domain. J. Mol. Biol. 311, 373–393.
[4] Kanelis, V., Bruce, M.C., Skrynnikov, N.R., Rotin, D. and Forman-Kay, J.D. (2006) Structural determinants for high-affinity

binding in a Nedd4 WW3* domain-Comm PY motif complex. Structure 14, 543–553.
[5] Nguyen, H., Jager, M., Kelly, J.W. and Gruebele, M. (2005) Engineering a beta-sheet protein toward the folding speed limit J Phys Chem B Condens Matter Mater Surf Interfaces. Biophys. 109, 15182–15186.
[6] Kay, B.K., Williamson, M.P. and Sudol, M. (2000) The importance of being proline: the interaction of proline-rich motifs in signaling proteins with their cognate domains. Faseb J. 14, 231–241.
[7] Sudol, M. and Hunter, T. (2000) NeW wrinkles for an old domain. Cell 103, 1001–1004.
[8] Sudol, M., Sliwa, K. and Russo, T. (2001) Functions of WW domains in the nucleus. FEBS Lett. 490, 190–195.
[9] Tapon, N., Harvey, K.F., Bell, D.W., Wahrer, D.C., Schiripo, T.A., Haber, D.A. and Hariharan, I.K. (2002) Salvador promotes both cell cycle exit and apoptosis in Drosophila and is mutated in human cancer cell lines. Cell 110, 467–478.
[10] Bairoch, A. and Boeckmann, B. (1991) The SWISS-PROT protein sequence data bank. Nucleic Acids Res. 19 (Suppl.), 2247–2249.
[11] Koepf, E.K., Petrassi, H.M., Ratnaswamy, G., Huff, M.E., Sudol, M. and Kelly, J.W. (1999) Characterization of the structure and function of W – > F WW domain variants: identification of a natively unfolded protein that folds upon ligand binding. Biochemistry 38, 14338–14351.
[12] Kigawa, T., Yabuki, T., Yoshida, Y., Tsutsui, M., Ito, Y., Shibata, T. and Yokoyama, S. (1999) Cell-free production and stable-isotope labeling of milligram quantities of proteins. FEBS Lett. 442, 15–19.
[13] Yokoyama, S. et al. (2000) Structural genomics projects in Japan. Nat. Struct. Biol. 7 (Suppl.), 943–945.
[14] Tochio, N. et al. (2006) Solution structure of the SWIRM domain of human histone demethylase LSD1. Structure 14, 457–468.
[15] Zwahlen, C., Legault, P., Vincent, S.J.F., Greenblatt, J., Konrat, R. and Kay, L.E. (1997) Methods for measurement of intermolecular NOEs by multinuclear NMR spectroscopy: application to a bacteriophage N-peptide/boxB RNA complex. J. Am. Chem. Soc. 119, 6711–6721.
[16] Delaglio, F., Grzesiek, S., Vuister, G.W., Zhu, G., Pfeifer, J. and Bax, A. (1995) NMRPipe: a multidimensional spectral processing system based on UNIX pipes. J. Biomol. NMR 6, 277–293.
[17] Johnson, B.A. and Blevins, R.A. (1994) NMR view: a computer program for the visualization and analysis of NMR data. J Biomol NMR. 4, 603–614.
[18] Herrmann, T., Güntert, P. and Wüthrich, K. (2002) Protein NMR structure determination with automated NOE-identification in the NOESY spectra using the new software ATNOS. J. Biomol. NMR 24, 171–189.
[19] Güntert, P., Mumenthaler, C. and Wüthrich, K. (1997) Torsion angle dynamics for NMR structure calculation with the new program DYANA. J. Mol. Biol. 273, 283–298.
[20] Güntert, P. (2004) Automated NMR structure calculation with CYANA. Methods Mol. Biol. 278, 353–378.
[21] Jee, J. and Güntert, P. (2003) Influence of the completeness of chemical shift assignments on NMR structures obtained with automated NOE assignment. J. Struct. Funct. Genom. 4, 179–189.
[22] Cornilescu, G., Delaglio, F. and Bax, A. (1999) Protein backbone angle restraints from searching a database for chemical shift and sequence homology. J. Biomol. NMR 13, 289–302.
[23] Cornell, W.D. et al. (1995) A second generation force field for the simulation of proteins, nucleic acids, and organic molecules. J. Am. Chem. Soc. 117, 5179–5197.
[24] Koradi, R., Billeter, M. and Güntert, P. (2000) Point-centered domain decomposition for parallel molecular dynamics simulation. Comput. Phys. Commun. 124, 139–147.
[25] Luginbuhl, P., Güntert, P., Billeter, M. and Wüthrich, K. (1996) The new program OPAL for molecular dynamics simulations and energy refinements of biological macromolecules. J. Biomol. NMR 8, 136–146.
[26] Laskowski, R.A., Rullmann, J.A., MacArthur, M.W., Kaptein, R. and Thornton, J.M. (1996) AQUA and PROCHECK-NMR: programs for checking the quality of protein structures solved by NMR. J. Biomol. NMR 8, 477–486.
[27] Koradi, R., Billeter, M. and Wüthrich, K. (1996) MOLMOL: a program for display and analysis of macromolecular structures. J. Mol. Graph. 14, 51–55, 29–32.
[28] Macias, M.J., Gervais, V., Civera, C. and Oschkinat, H. (2000) Structural analysis of WW domains and design of a WW prototype. Nat. Struct. Biol. 7, 375–379.
[29] Nilges, M. (1995) Calculation of protein structures with ambiguous distance restraints. Automated assignment of ambiguous NOE crosspeaks and disulphide connectivities. J. Mol. Biol. 245, 645–660.
[30] Ash, E.L. et al. (2000) Unusual 1H NMR chemical shifts support (His) C(epsilon) 1···O═C H-bond: proposal for reaction-driven ring flip mechanism in serine protease catalysis. Proc. Natl. Acad. Sci. USA 97, 10371–10376.
[31] Day, R.M. et al. (2003) Tautomerism, acid–base equilibria, and H-bonding of the six histidines in subtilisin BPN' by NMR. Protein Sci. 12, 794–810.
[32] Sudmeier, J.L. et al. (2003) Identification of histidine tautomers in proteins by 2D $^{1}H/^{13}C^{\delta 2}$ one-bond correlated NMR. J. Am. Chem. Soc. 125, 8430–8431.
[33] Udan, R.S., Kango-Singh, M., Nolo, R., Tao, C. and Halder, G. (2003) Hippo promotes proliferation arrest and apoptosis in the Salvador/Warts pathway. Nat. Cell Biol. 5, 914–920.
[34] Creasy, C.L., Ambrose, D.M. and Chernoff, J. (1996) The Ste20-like protein kinase, Mst1, dimerizes and contains an inhibitory domain. J. Biol. Chem. 271, 21049–21053.
[35] Sonnhammer, E.L., Eddy, S.R. and Durbin, R. (1997) Pfam: a comprehensive database of protein domain families based on seed alignments. Proteins 28, 405–420.